time scales of ~6 min, implying structure on scales of less than 10 km.

Methane lost from the upper atmosphere of Titan because of photo dissociation has to be replenished either from a large reservoir on the surface in the form of oceans or episodically as a result of volcanic activity, for example. A detailed knowledge of Titan's surface can address this issue and is the key to understanding the history of Titan's atmosphere.

References and Notes

1. D. O. Muhleman, A. W. Grossman, B. J. Butler, M. A. Slade, *Science* **248**, 975 (1990).
2. J. I. Lunine, D. J. Stevenson, Y. L. Yung, *Science* **222**, 1229 (1983).
3. P. H. Smith, M. T. Lemmon, R. D. Lorenz, L. A. Sromovsky, J. J. Calwell, M. D. Allison, *Icarus* **119**, 336 (1996).
4. S. G. Gibbard *et al.*, *Icarus* **139**, 189 (1999).
5. R. Meier, B. A. Smith, T. C. Owen, R. J. Terrile, *Icarus* **145**, 462 (2000).
6. A. Coustenis, E. Lellouch, J. P. Maillard, C. P. McKay, *Icarus* **118**, 87 (1995).
7. C. A. Griffith, T. Owen, T. R. Geballe, J. Rayner, P. Rannou, *Science* **300**, 628 (2003).
8. D. B. Campbell, J. F. Chandler, S. J. Ostro, G. H. Pettengill, I. I. Shapiro, *Icarus* **34**, 254 (1978).
9. S. J. Ostro *et al.*, *J. Geophys. Res.* **97**, 18227 (1992).
10. C. A. Griffith, T. Owen, G. A. Miller, T. Geballe, *Nature* **395**, 575 (1998).
11. The uniform spacing of the sixteen 2001 spectra allows the diffuse component to be partially deconvolved so that each resultant spectrum more closely represents the diffuse scattering from a limited range of longitudes. There is no change in the amplitude or shape of the specular echoes. When estimating the diffuse cross section of the bright region, this process compensates for its limited extent in longitude. Its limited extent in latitude was compensated for by assuming that the surface south of the bright region has the same scattering properties as the trailing hemisphere. The deconvolution has the effect of symmetrizing the diffuse spectra, making the detection of a weak specular echo in the fits much easier.
12. R. D. Lorenz, S. E. Shandera, *Geophys. Res. Lett.* **28**, 215 (2001).
13. C. Sagan, S. F. Dermott, *Nature* **300**, 731 (1982).
14. W. R. Thompson, S. W. Squyres, *Icarus* **86**, 336 (1990).
15. For smooth dielectric spheres, the (specular) radar cross section is a measure of the Fresnel reflectivity. This relation still holds to a close approximation for slightly roughened dielectric spheres that are smooth at the scale of the radar wavelength but have large-scale slopes (*20*). Because the Fresnel reflectivity (ρ_o) and the relative dielectric constant (ε) are related by $\rho_o = |(\sqrt{\varepsilon} - 1)/(\sqrt{\varepsilon} + 1)|^2$, a good estimate of ε can be obtained from a measurement of the specular cross section.
16. Fits of combined specular and diffuse scattering laws were made to the individual spectra. The diffuse law was of the form $\sigma_o(\theta) = A\cos^n\theta$, where $\sigma_o(\theta)$ is the backscatter cross section per unit surface area at the incidence angle θ. The specular law used was Hagfors' formulation, $\sigma_o(\theta) = \rho_o C/2[\cos^4\theta + C \sin^2\theta]^{-3/2}$, where $C^{-1/2}$ is the (undulating) surface RMS slope (*21*).
17. N. A.-L. Ghafoor, J. C. Zarnecki, P. C. Challenor, M. A. Srokosz, *J. Geophys. Res.* **105**, 12077 (2000).
18. R. D. Lorenz, *Icarus* **136**, 344 (1998).
19. S. Rodriguez *et al.*, *Icarus* **164**, 213 (2003).
20. J. V. Evans, T. Hagfors, *Radar Astronomy* (McGraw-Hill, New York, 1968), chap. 4.
21. T. Hagfors, *J. Geophys. Res.* **66**, 3779 (1964).

22. We thank A. Hine, A. Crespo, R. French, J-L. Margot, M. Nolan, P. Nicholson, P. Perillat, and the staffs of the Arecibo and Green Bank telescopes. J. Chandler and J. Giorgini provided the Titan observing ephemeredes. Extensive comments by C. Griffith, one of which is paraphrased in the last paragraph, are appreciated. D.B.C., L.M.C., and S.J.O. acknowledge support by the Planetary Astronomy and Planetary Geology and Geophysics Programs of the National Aeronautics and Space Administration (NASA). Part of this research was conducted at the Jet Propulsion Laboratory, California Institute of Technology, under contract with NASA. The Arecibo Observatory is part of the National Astronomy and Ionosphere Center, which is operated by Cornell University under a cooperative agreement with the National Science Foundation (NSF) and with support from NASA. The Green Bank Telescope is part of the National Radio Astronomy Observatory, a facility of the NSF operated under cooperative agreement by Associated Universities, Inc.

9 July 2003; accepted 22 September 2003
Published online 2 October 2003;
10.1126/science.1088969
Include this information when citing this paper.

Contribution of the Patagonia Icefields of South America to Sea Level Rise

Eric Rignot,[1]* Andrés Rivera,[2,3]* Gino Casassa[3]*

Digital elevation models of the Northern and Southern Patagonia Icefields of South America generated from the 2000 Shuttle Radar Topography Mission were compared with earlier cartography to estimate the volume change of the largest 63 glaciers. During the period 1968/1975–2000, these glaciers lost ice at a rate equivalent to a sea level rise of 0.042 ± 0.002 millimeters per year. In the more recent years 1995–2000, average ice thinning rates have more than doubled to an equivalent sea level rise of 0.105 ± 0.011 millimeters per year. The glaciers are thinning more quickly than can be explained by warmer air temperatures and decreased precipitation, and their contribution to sea level per unit area is larger than that of Alaska glaciers.

The Northern Patagonia Icefield (NPI), located completely in Chile, and the Southern Patagonia Icefield (SPI), shared between Chile and Argentina, are the largest temperate ice masses in the Southern Hemisphere (*1*). They cover an area of 4200 and 13,000 km^2 (*2*, *3*), respectively; receive abundant precipitation (2 to 11 m of water equivalent per year), with a large east-west gradient; and discharge ice and meltwater to the ocean on the west side and to lakes on the east side via rapidly flowing glaciers (*4*). Few reliable mass balance data on the region exist, leaving considerable uncertainty in the estimation of its contribution to sea level rise (SLR) (*5*–*9*). The fronts of most of these glaciers have been retreating over the past half century or more, and discrete measurements of thickness change in the ablation area of a few glaciers indicate rapid thinning (*8*). Yet the existing data have not been sufficient to get an accurate estimate of the total volume loss. Here we report an estimation of volume loss over the entire area of the icefields, based on a direct method.

In February 2000, NASA and the U.S. Department of Defense's National Imaging and Mapping Agency (NIMA) flew the Shuttle Radar Topography Mission (SRTM) to provide the first global topographic coverage of Earth between latitudes +60°N and 57°S. The data were processed into continental maps, with global positioning system (GPS) control, 7-m vertical precision, and 90-m horizontal posting (*10*), to provide the first comprehensive and systematic topographic coverage of Patagonia (Fig. 1). A comparison of SRTM data with GPS surface reference data on Tyndall (*11*) and Chico (*12*) Glaciers indicates local systematic vertical errors of –3 m and +4.5 m, which is consistent with the 7-m vertical precision of SRTM and with negligible biases from the penetration of radar signals into snow and ice (*13*).

Prior digital elevation models (DEMs) of NPI and SPI were assembled from maps compiled by the Instituto Geográfico Militar of Chile (IGMCh) and Argentina. Aerial photographs from March 1975 produced the first regular cartography by photogrammetric restitution, including analog analysis of the photographs and plotting of contour lines from stereo models in areas with adequate stereoscopic views. In May 1995,

[1]Jet Propulsion Laboratory, California Institute of Technology, MS 300–227, Pasadena, CA 91109–8099, USA. [2]Departamento de Geografía, Universidad de Chile, Santiago, Chile; and University of Bristol, School of Geographical Sciences, University Road, BS8 1SS, Bristol, UK. [3]Centro de Estudios Científicos, Valdivia, Chile.

*To whom correspondence should be addressed. E-mail: eric.rignot@jpl.nasa.gov (E.R.); andres.rivera@bristol.ac.uk (A.R.); gcasassa@cecs.cl (G.C.)

IGMCh made a second regular cartography for most of SPI, using digital photogrammetric procedures to cover with contour lines areas with poor stereoscopic views or not mapped in 1975. To complement these data, we used Argentinean cartography from 1968 along the eastern side of SPI. DEMs generated from the cartography have a vertical precision of 19 m for the IGMCh data and 50 m for the Argentinean data (*14*, *15*).

The thinning rates measured at low elevation during 1968/1975–2000 (Fig. 2) are several standard deviations larger than the uncertainty of measurement (*16*). Thinning varies significantly with elevation. Above 1200 m, the signal falls within the measurement error, and a large fraction (75%) of the accumulation area is not covered by contour lines in the 1975 IGMCh topography. Glacier thinning is observed well above the equilibrium line altitude (ELA) of SPI glaciers (table S1) and at the ELA of NPI glaciers, however, suggesting that thinning affects most of the high plateau accumulation area.

Elevation changes measured at low elevations near the central flow line were fitted to a third-order polynomial as a function of elevation to extrapolate the results to higher elevations, imposing the boundary condition that thinning drops slowly to zero at the highest elevations, and eliminating measurements deviating by more than a few standard deviations from the local mean at low elevations. Model fitting is justified by the similarity in ice thinning with that observed in Alaska: an exponential decay of thinning with elevation and little thinning at high elevation (*17*). Few field data are available in the accumulation area to quantify the uncertainty of our extrapolation, but existing data indicate thinning. Aniya (*8*) reports qualitative evidence for ice thinning of 0.5 to 1 m/year in the accumulation area of Soler and Arenales (NPI). Rivera (*12*) measured meter-scale ice thinning in the accumulation area of Chico (SPI), using differential GPS data. Meteorological data suggest that precipitation has changed little over NPI in the past four decades but may have decreased 5% on SPI (*18*), which is equivalent to a thinning of 0.38 m/year of ice if we assume a mean accumulation rate of 7 m/year of water for SPI (*4*).

Many glaciers experienced significant frontal retreat between 1968/1975 and 2000 (*2*–*4*). Volume loss includes glacier thinning over the year 2000 glacier basin and frontal loss associated with glacier retreat at the front, tributary branches, and ice margins since 1968/1975. We find that volume loss by glacier thinning is 4 to 10 times larger than that by frontal loss (table S1). In NPI, the glacier thinning of 24 glaciers is 2.63 ± 0.4 km^3/year over an area of 3481 km^2, with a frontal loss of 0.20 km^3/year. Scaled over the entire icefield of 4200 km^2 (*3*), this implies a volume loss of 3.2 ± 0.4 km^3/year. During the same period, SPI glaciers lost 7.2 ± 0.5 km^3/year over an area of 8167 km^2 and an additional 1.3 km^3/year frontal loss. Scaled over the entire icefield of 13,000 km^2 (*2*), this implies a loss of 13.5 ± 0.8 km^3/year of ice. The total volume loss of NPI and SPI of 16.7 ± 0.9 km^3/year is equivalent to a SLR of 0.042 ± 0.002 mm/year, with an ice density

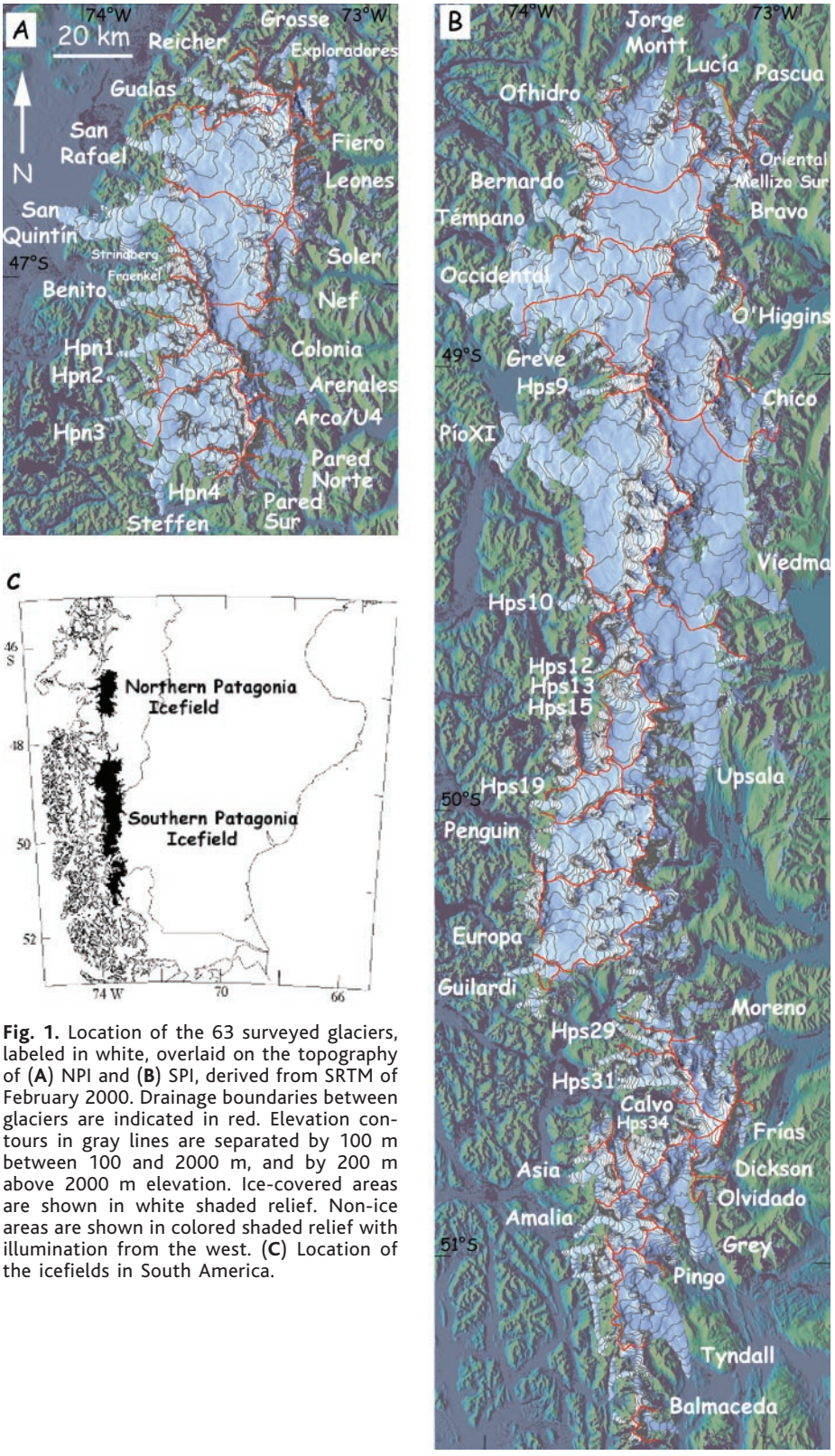

Fig. 1. Location of the 63 surveyed glaciers, labeled in white, overlaid on the topography of (**A**) NPI and (**B**) SPI, derived from SRTM of February 2000. Drainage boundaries between glaciers are indicated in red. Elevation contours in gray lines are separated by 100 m between 100 and 2000 m, and by 200 m above 2000 m elevation. Ice-covered areas are shown in white shaded relief. Non-ice areas are shown in colored shaded relief with illumination from the west. (**C**) Location of the icefields in South America.

of 900 kg/m^3. This result agrees with earlier rough estimates (*8*, *9*).

The area-average thinning rate is 1.0 ± 0.1 m/year (table S1), with 25% larger values on SPI than NPI (Fig. 2), which is consistent with existing field data (*8*). Thinning near the glacier snout ranges from 1 to 8 m/year on NPI, and –2 (Pío XI) to 18 m/year (Jorge Montt) on SPI. Glaciers on the northern half of SPI thinned more rapidly than those on the southern half. Several large glaciers experienced massive thinning (Jorge Montt, Greve, Amalia, Dickson, Upsala, and O'Higgins) and retreated several kilometers, which is comparable in magnitude to the rapid retreat of Columbia Glacier in Alaska (*19*).

A similar analysis was applied on a limited area of SPI, where 1995 cartography was available to us, showing a larger noise level due to the shorter time separation (Fig. 2). On glaciers for which both 1975 and 1995 cartography were available, we detect a large increase in thinning rates (table S1). Glacier thinning over an area of 5642 km^2 was 14.3 ± 1.9 km^3/year in 1995–2000. Assuming the same rate of frontal loss as in 1975–2000, we calculate a volume loss of 38.7 ± 4.4 km^3/year for SPI. Assuming no accelerated thinning on NPI, the volume loss from both icefields is 41.9 ± 4.4 km^3/year, which is equivalent to a SLR of 0.105 ± 0.011 mm/year.

Pío XI is the only large advancing glacier in SPI. It thickened between 1975 and 2000 at low elevations and thinned between 1995 and 2000 at high elevations (table S1). We attribute this trend to the surging of the glacier in recent decades (*20*), which displaced a large ice mass from upper elevations to lower elevations, resulting in thickening and frontal advance at low elevations and thinning in the accumulation area. Pío XI started retreating after 1997. Overall, the glacier is likely to have been thinning.

Ice thinning is largest on HPS12 (>28 m/year), which experienced a catastrophic retreat in the late 1990s. Many glaciers more than doubled their thinning rate in recent years (table S1). In situ measurements of elevation changes on Tyndall Glacier indicate an increase of the thinning rates in the late 1980s from 1.9 m/year for 1945 to 1975, to 3.3 m/year for 1985 to 2002 (*11*). Ice thinning also increased on Upsala Glacier from 3.6 m/year near the front for 1968 to 1990, to 11 m/year for 1990 to 1993 (*21*, *22*). Conversely, O'Higgins Glacier, which showed the largest retreat (14 km) of all Patagonia glaciers in this century (*23*), slowed its retreat in recent years (*8*) and thinned less rapidly (table S1), possibly because of shallower fjord depths at O'Higgins Lake, which resulted in increased flow drag and lower calving activity. Moreno Glacier is the only glacier experiencing little to no thinning (Fig. 2 and table S1).

The primary cause for the thinning of Patagonia glaciers must be a negative mass balance caused by climate change. Long-term changes in temperature suggest a 0.4° to 1.4°C temperature increase in this century south of 46°S (*24*), with temperature increases being higher southward, which explains the higher thinning rates of SPI as compared to NPI (table S1). Over the past 40 years, temperature increased 0.5°C at 850 mb, which is near the ELA (*18*). A 0.3°C warming in 25 years would raise the ELA by 50 m, based on a lapse rate of 0.6°C/100 m. If we accept a steady-state mass balance change of 0.015/year for the ablation area (*25*), an increase in melt of 50 × 0.015 = 0.75 m/year is calculated. Melt will further increase from topography feedback, as the glacier surface lowers with time, by 0.75 × 25 × 0.015 = 0.28 m/year. Combining this 1 m/year thinning of the ablation area of SPI (4100 km^2) with a 0.38 m/year decrease in precipitation (*18*, *26*, *27*) over the accumulation area (8700 km^2) yields a negative mass balance of 0.6 m/year, which is half of the observed signal in 1975–2000. Climate forcing due to warmer and drier conditions is therefore not sufficient to explain the glacier thinning rates.

A large fraction of the NPI and SPI outlet glaciers are calving glaciers (*28*), versus only a few in Alaska. Twice as many calve in fresh water as in tidewater (table S1). Calving glaciers are more sensitive to climate change than noncalving glaciers, and once pushed out of equilibrium by climate, they can undergo large aclimatic changes controlled mainly by their calving dynamics (*29*). Climate warming and drier conditions alone cannot explain the area-average thinning rates of the major glaciers [Occidental (2.2 m/year), O'Higgins (1.5 m/year), and Jorge Montt (3.3 m/year)], which dominate the icefield mass budget (table S1). A substantial part of the thinning must be due to ice dynamics, which means excess creep (ice thinning from longitudinal stretching) and accelerated calving (ice loss to the ocean or lakes). Climate warming enhances meltwater production, which in turn increases basal lubrication and allows faster flow rates, as recently revealed on Soler Glacier (*30*). As calving glaciers retreat from stabilizing morainal shoals or bed rises, calving accelerates and entrains the glaciers further into a recession (*19*, *23*, *25*).

The Patagonia glaciers cover an area five times smaller than their Alaskan counterparts (90,000 km^2), yet they account for 9% of the SLR contribution from mountain glaciers (*5*) versus 30% in Alaska. The contribution of Patagonia to SLR is therefore disproportionately larger (by a factor of 1.5) than is indicated by its area. We attribute this enhanced vulnerability of Patagonia glaciers to climate change to their higher turnover rates and low ELAs, combined with the dominance of calving glaciers.

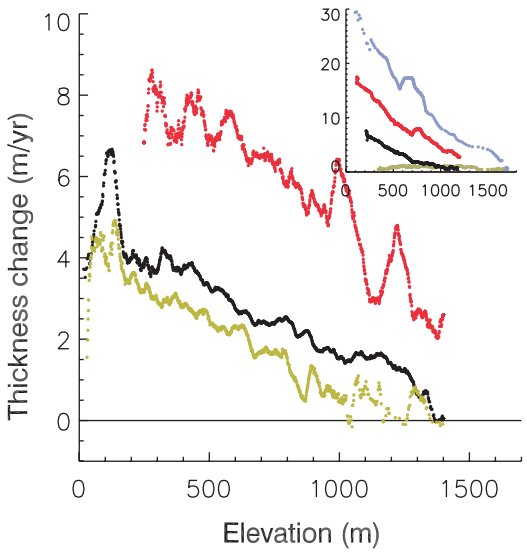

Fig. 2. Thickness change versus elevation of NPI (brown, 24 glaciers) and SPI (black, 31 glaciers) during the 1975–2000 period and the 1995–2000 period (SPI, red, 20 glaciers). Each plot is the average of all glaciers. The decrease in thinning at low elevations occurs because ice was completely removed at the ice front. The average of all glaciers includes too few data points above 1400 m elevation. The inset shows the thinning rate measured along the central flow line of glaciers HPS 12 (1995–2000, light blue), Jorge Montt (1975–2000, red), Upsala (1968–2000, black), and Moreno (1975–2000, brown) (table S1).

References and Notes

1. C. R. Warren, D. E. Sudgen, *Arct. Alp. Res.* **25**, 316 (1993).
2. M. Aniya, H. Sato, R. Naruse, P. Skvarca, G. Casassa, *Photogram. Eng. Remote Sens.* **62**, 1361 (1996).
3. M. Aniya, *Arct. Alp. Res.* **20**, 179 (1988).
4. G. Casassa, A. Rivera, M. Aniya, R. Naruse, in *The Patagonian Icefields: A Unique Natural Laboratory for Environmental and Climate Change Studies*, G. Casassa, F. Sepúlveda, R. Sinclair, Eds. (Kluwer Academic/Plenum, New York, 2002), pp. 67–83.
5. M. F. Meier, *Science* **226**, 1419 (1984).
6. M. B. Dyurgerov, *INSTAAR Occasional Paper 55* (Univ. of Colorado, Boulder, CO, 2002).
7. W. Haeberli, R. Frauenfelder, M. Hoelzle, M. Maisch, *Geogr. Ann. Phys. Geogr.* **81A**, 585 (1999).
8. M. Aniya, *Arct. Antarct. Alp. Res.* **31** 165 (1999).
9. A. Rivera, C. Acuña, G. Casassa, F. Brown, *Ann. Glaciol.* **34**, 367 (2002).
10. S. Hensley, P. Rosen, E. Gurrola, in *Proceedings of*

SPIE, Volume 4152, Microwave Remote Sensing of the Atmosphere and Environment II, Sendai, Japan, 9 to 12 October 2000, T. T. Wilheit, H. Masuko, H. Wakabayashi, Eds. (SPIE, Sendai, Japan, 2000).
11. C. Raymond, T. Neumann, E. Rignot, A. Rivera, G. Casassa, *EOS* **81** (fall meeting supplement), H61G02 (2000).
12. A. Rivera, unpublished data.
13. E. Rignot, K. Echelmeyer, W. B. Krabill, *Geophys. Res. Lett.* **28**, 3501 (2001).
14. A. Rivera, "Comparison of DEMs generated from topographic maps of 1975 and 1995" (Bristol Glaciology Centre, Bristol, UK, 2001) (unpublished).
15. The 1995 cartography has not been published, but IGMCh permitted restricted access to the cartography for the lower reaches of a few SPI glaciers. The DEMs were generated by interpolation of 50-m contour lines digitized from the available cartography, using a discretized thin plate spline interpolation. The 1975 DEM covers both icefields, mostly at the lower elevation [<1200 m (table S1)] because of the lack of recognizable surface features in the photographs at the higher elevation glacier plateau. The 1995 DEM only covers SPI and does not include all the glacier fronts. The DEMs are referenced to mean sea level with a World Geodetic System 1984 datum. The vertical precision of the DEMs is 19 m (17 m error in regular cartography, and 9 m error in contour interpolation). No information is available about the precision of the Argentinean cartography, but comparison with SRTM on exposed rock reveals a vertical random error of 50 m near Chico, Viedma, and Upsala Glaciers and larger errors to the north, south, and west of these regions, where the cartography is not reliable.
16. The random error in elevation difference with SRTM is 20 m for the 1975/1995 DEMs and 50 m for the 1968 DEM. The extrapolation error of the elevation changes due to polynomial fitting was calculated for each glacier as the standard error of the model fit (1σ) and ranges from 10 to 30 m. The total error is the quadrature sum of these two errors. For area-average thickness changes, the total error is further divided by the square root of the number of IGMCh contours employed, typically around 20, depending on the glacier coverage by IGMCh and its area-elevation distribution (table S1). Few contours are available on the accumulation plateau.
17. A. Arendt, K. A. Echelmeyer, W. D. Harrison, C. S. Lingle, V. B. Valentine, *Science* **297**, 382 (2002).
18. L. A. Rasmussen, H. Conway, C. F. Raymond, in preparation.
19. M F. Meier, M. B. Dyurgerov, *Science* **297**, 350 (2002).
20. A. Rivera, G. Casassa, *Global Planet. Change* **22**, 233 (1999).
21. M. Aniya, H. Sato, R. Naruse, P. Skvarca, G. Casassa, *Arct. Alp. Res.* **29**, 1 (1997).
22. P. Skvarca, K. Satow, R. Naruse, J. Leiva, *Bull. Glacier Res.* **13**, 11 (1995).
23. G. Casassa, H. Brecher, A. Rivera, M. Aniya, *Ann. Glaciol.* **24**, 106 (1997).
24. B. Rosenblüth, H. A. Fuenzalida, P. Aceituno, *Int. J. Climatol.* **17**, 67 (1997).
25. R. Naruse, M. Aniya, P. Skvarca, G. Casassa, *Ann. Glaciol.* **21**, 297 (1995).
26. T. Ibarzabal y Donángelo, J. Hoffmann, R. Naruse, *Bull. Glacier Res.* **14**, 29 (1996).
27. J. Carrasco, G. Casassa, A. Rivera, in *The Patagonian Icefields: A Unique Natural Laboratory for Environmental and Climate Change Studies*, G. Casassa, F. Sepúlveda, R. Sinclair, Eds. (Kluwer Academic/Plenum, New York, 2002), pp. 29–41.
28. C. Warren, M. Aniya, *Global Planet. Change* **22**, 59 (1999).
29. M. F. Meier, A. Post, *J. Geophys. Res.* **92**, 9051 (1987).
30. S. Yamaguchi, R. Naruse, T. Matsumoto, H. Ohno, *Arct. Antarct. Alp. Res.* **35**, 170 (2003).
31. We thank the Jet Propulsion Laboratory (JPL) processing team for the SRTM data; IGMCh for providing restricted access to the cartography of the icefields; M. Peña for his assistance in digitizing contour lines of the icefields; and L. Rasmussen, H. Conway, and C. Raymond for sharing their results in advance of publication. E.R. performed this work at JPL under a contract with NASA's Solid Earth and Natural Hazard Program. A.R. was supported by Fondo Nacional de Ciencia y Tecnología, Chile project 1000445.

Supporting Online Material

www.sciencemag.org/cgi/content/full/302/5644/434/DC1

Table S1

References and Notes

29 May 2003; accepted 23 September 2003

The Chemistry of Sexual Deception in an Orchid-Wasp Pollination System

Florian P. Schiestl,[1]* Rod Peakall,[1] Jim G. Mant,[1]* Fernando Ibarra,[2] Claudia Schulz,[2] Stephan Franke,[2] Wittko Francke[2]†

The "sexually deceptive" orchid *Chiloglottis trapeziformis* attracts males of its pollinator species, the thynnine wasp *Neozeleboria cryptoides*, by emitting a unique volatile compound, 2-ethyl-5-propylcyclohexan-1,3-dione, which is also produced by female wasps as a male-attracting sex pheromone.

Despite the large number and wide variety of animal pollinated plants, as well as the crucial role of floral volatiles in pollinator attraction (*1*), little is known about the attractiveness of volatile compounds to specific pollinators (*2*, *3*). In most cases where pollinator-attracting substances have been identified, they proved to be mixtures of rather common compounds (*4*, *5*). In sexually deceptive orchids, in which the flowers mimic female insects, a combination of ethological and chemical investigations have shown that floral volatiles are responsible for the attraction of specific pollinators (*6*–*9*). In such cases, floral volatiles are a key trait for the reproductive isolation of sympatric species and play a major role in the evolutionary dynamics of sexually deceptive orchid lineages (*10*).

The Australian orchid genus *Chiloglottis* relies exclusively on sexual deception for pollination (*7*). We investigated *C. trapeziformis* Fitzg. and its pollinator, the thynnine wasp *Neozeleboria cryptoides* (Smith). To identify the specific compound(s) attracting males to flowers (pollination) and to female wasps (mate finding), we analyzed labella extracts of the orchid and head extracts of female wasps (*11*). Gas chromatography (GC) coupled with electroantennographic detection (GC-EAD) (*11*, *12*), using antennae of *N. cryptoides* males, revealed only one single component to be biologically active. This compound proved to be identical in orchids and wasps.

Elucidation of the structure of the target compound was based predominantly on GC-mass spectroscopy (GC-MS), GC coupled with Fourier transform infrared (FT-IR) spectroscopy, and microreactions, as the samples contained too little material even for modern

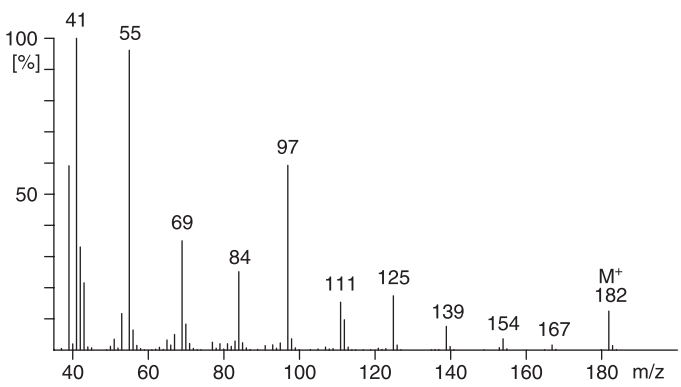

Fig. 1. 70V EI-mass spectrum of 2-ethyl-5-propylcyclohexan-1,3-dione.

[1]School of Botany and Zoology, The Australian National University, Canberra ACT 0200, Australia. [2]Institute of Organic Chemistry, University of Hamburg, Martin-Luther-King Platz 6, D-20146 Hamburg, Germany.

*Present address: Geobotanical Institute, ETH Zürch, Zollikerstrasse 107, CH-8008 Zürich, Switzerland.

†To whom correspondence should be addressed. E-mail: francke@chemie.uni-hamburg.de